Cell Reports

Article

Non-homogenous axonal bouton distribution in whole-brain single-cell neuronal networks

Graphical abstract

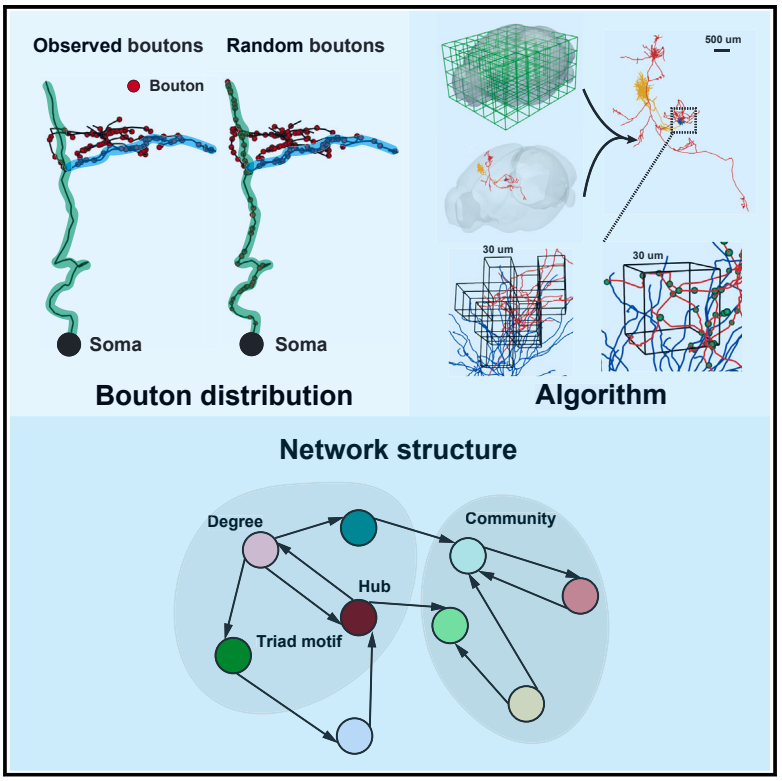

Authors

Penghao Qian, Linus Manubens-Gil, Shengdian Jiang, Hanchuan Peng

Correspondence

linusmg@seu.edu.cn (L.M.-G.), h@braintell.org (H.P.)

In brief

Qian et al. examined the pre-synaptic contacts distribution in mouse neurons' axons and constructed whole-brain single-cell neuronal networks. They found that bouton distributions were not homogeneous, having a significant impact on network wiring. The results suggest that neuroanatomical details must be carefully addressed in single-cell-level network analyses.

Highlights

- Accounting for axonal bouton distributions is necessary to determine network topology
- Single-neuron morphological details are main contributors to network connectivity
- Detailed network analysis using 1,891 full morphology tracings and putative bouton datasets

Qian et al., 2024, Cell Reports *43*, 113871
March 26, 2024
https://doi.org/10.1016/j.celrep.2024.113871

CellPress

Cell Reports

CellPress
OPEN ACCESS

Article

Non-homogenous axonal bouton distribution in whole-brain single-cell neuronal networks

Penghao Qian,[1,2,3] Linus Manubens-Gil,[1,3,4,*] Shengdian Jiang,[1,2] and Hanchuan Peng[1,*]
[1]New Cornerstone Science Laboratory, SEU-ALLEN Joint Center, State Key Laboratory of Digital Medical Engineering, Institute for Brain and Intelligence, Southeast University, Nanjing, Jiangsu 210096, China
[2]School of Computer Science and Engineering, Southeast University, Nanjing, Jiangsu 210096, China
[3]These authors contributed equally
[4]Lead contact
*Correspondence: linusmg@seu.edu.cn (L.M.-G.), h@braintell.org (H.P.)
https://doi.org/10.1016/j.celrep.2024.113871

SUMMARY

We examined the distribution of pre-synaptic contacts in axons of mouse neurons and constructed whole-brain single-cell neuronal networks using an extensive dataset of 1,891 fully reconstructed neurons. We found that bouton locations were not homogeneous throughout the axon and among brain regions. As our algorithm was able to generate whole-brain single-cell connectivity matrices from full morphology reconstruction datasets, we further found that non-homogeneous bouton locations have a significant impact on network wiring, including degree distribution, triad census, and community structure. By perturbing neuronal morphology, we further explored the link between anatomical details and network topology. In our *in silico* exploration, we found that dendritic and axonal tree span would have the greatest impact on network wiring, followed by synaptic contact deletion. Our results suggest that neuroanatomical details must be carefully addressed in studies of whole-brain networks at the single-cell level.

INTRODUCTION

Neuronal morphology plays a fundamental role in determining the function of neuronal networks. Neurons are polarized cells conformed by the dendritic and axonal trees. Axons send connections to dendrites from other neurons through membrane specializations called synapses, which are structures that allow transmission of neuronal electrophysiological impulses. The architecture of the trees and the distribution of synapses within them determine the connectivity of neuronal networks. Changes in the structure of neurons can have a dramatic impact on cognition, and changes in dendrite shape and size have been associated with intellectual disability.[1] Previous work from our team showed how the detailed organization of post-synaptic contacts in dendritic trees shapes neuron firing.[2] However, understanding the effect of single-neuron morphology on whole-brain circuit connectivity is still an open challenge.

Limited by resolution and time cost, current studies on the structural properties of whole-brain connectivity are mostly described from the mesoscale and macroscale perspectives. Studies of human brain networks[3] using magnetic resonance imaging show that there is a functional division in the brain at the anatomical level,[4] called community structure.[5,6] This structure means that brain networks can be divided into subnetworks with specific cognitive functions,[7–12] with high-node-density communities and sparse communities connecting them.[5,13–15] Several experiments have also shown that the average path distance between nodes is much smaller in macroscopic brain networks than in random networks,[16–18] reflecting their small-world topology and the existence of central hubs.[19,20] This is thought to improve the segregation and integration of information within the brain,[21] reducing the cost associated with information processing.[22,23] However, most of the experimental data obtained in these studies consists of ~1 mm sided voxels, which pool information from thousands of individual neurons.

At the mesoscale, the Allen Institute for Brain Science conducted a comprehensive study of the mouse brain connectivity, mapping the whole brain using population-based tracer injections.[24] The study found that the clustering coefficients are close to those expected in a small-world network, while the degree distribution is close to a scale-free network.[24] A refined connectivity analysis of the same experimental data showed global hubs in the mouse brain, including associative cortical areas, dorsal portions of the hippocampus, and subregional portions of the basolateral and central amygdala.[25,26] The results also show highly connected central hub nodes interlinked with each other throughout the brain, supporting the efficient integration of otherwise segregated neural circuits. Neuromodulatory nuclei work as connector hubs and critical orchestrators of network communication at the fine granularity.[25] These studies have deepened our understanding of brain structure, but they still rely on measurements in large populations of tracer-injected neurons, missing the details of single-neuron morphologies. Therefore, it is necessary to study neuronal morphology on the single-cell level, as it is more meaningful in terms of finer and more essential brain network structures.

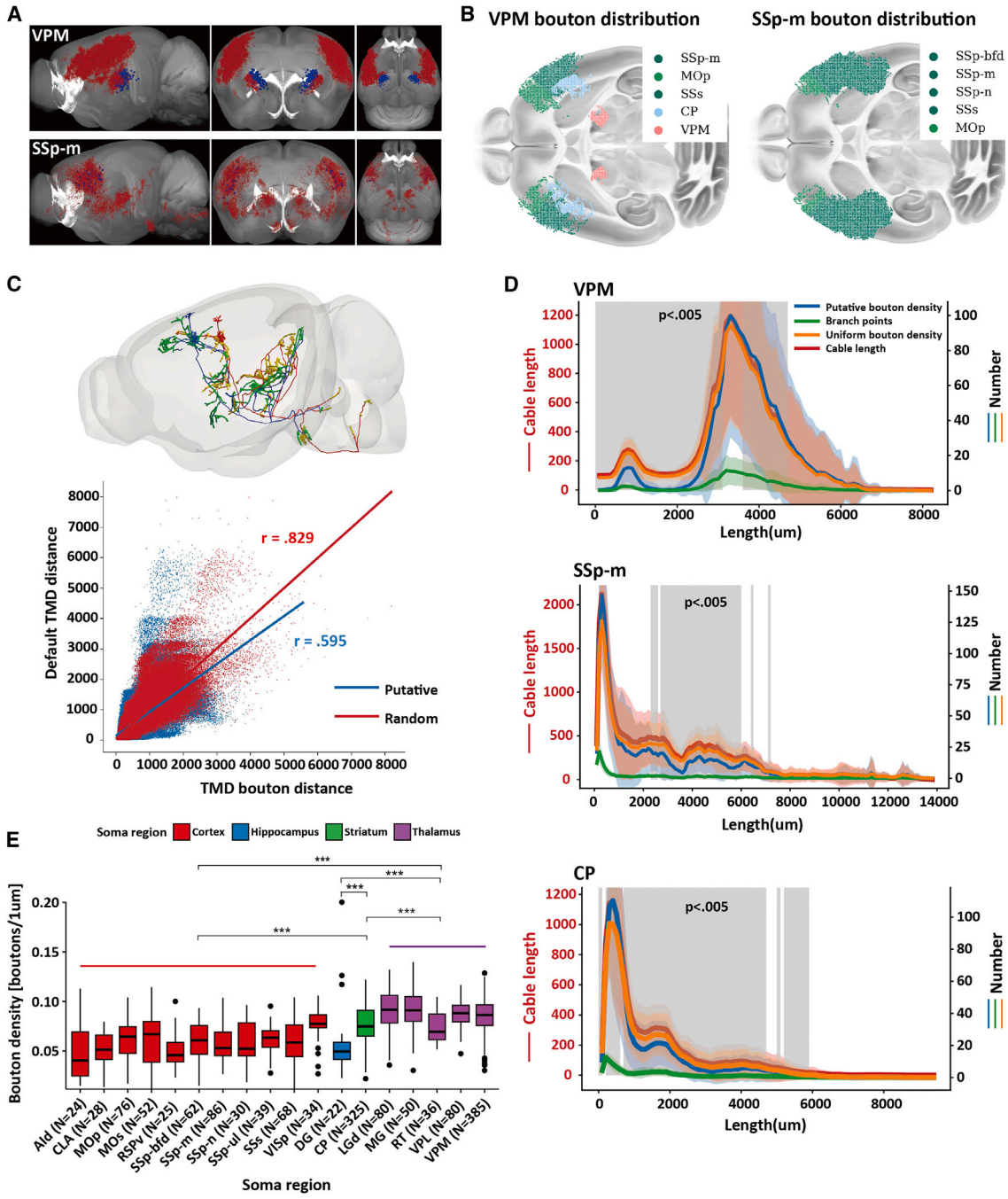

Figure 1. Axonal bouton distribution is cell-type dependent

(A) 2D sagittal, coronal, and horizontal projections of putative bouton locations (in red) from two sets of neurons with somas (in blue) located in the ventral posteromedial (VPM) nucleus of the thalamus (TH) and mouth primary somatosensory (SSp-m) area of the cortex based on the CCFv3 parcellation (N_{VPM} = 379, N_{SSp-m} = 78). See supporting datasets in the data and code availability section for a complete list of acronyms.

(B) Horizontal projection of bouton locations in the top five regions most innervated by VPM and SSp-m neurons. Cortical regions are colored in shades of green, caudoputamen (CP) in the striatum (STR) in blue, and VPM in the TH in pink.

(C) Top: morphologically similar neurons have analogous bouton distributions throughout the axons. Bottom: scatterplot of the topological morphology descriptor (TMD) distances between pairs of neurons with somas in the same region using default TMD (x axis) or TMD bouton (y axis; see STAR Methods). The plot shows pairwise distances for neurons with putative bouton locations (blue) and analogous measures for uniformly distributed boutons (red). "r" values specify Pearson correlation coefficients.

(D) Sholl analysis of the number of boutons, cable length, and density of boutons for neurons with their soma in VPM (top), SSp-m (middle), or CP (bottom). Lines indicate average values overlaid to shadows indiciating the standard error of the mean. When calculating boutons, we use the path distance to the soma instead

(legend continued on next page)

At the single-cell level, limited by the lack of experimental data, only a few studies have explored the impact of morphological details on whole-brain connectivity. Electron microscopy studies provide highly reliable data for the study of synaptic sites at the subcellular scale, but currently, those are limited to subregions of the mammal brain and do not allow direct extraction of brain circuit topology.[27] Alternatively, light microscopy approaches are being used to approximate brain circuit topology at the cellular scale. In a study of the hippocampal trisynaptic circuit, a highly specialized topology has been shown to minimize communication cost through information-processing hubs nested in a two-tier structure that manage the network traffic with strong resilience to random perturbations.[28] However, a recent study of bouton-spine pairs in the rat barrel cortex found that most overlapping axons and dendrites were not connected,[29] indicating that the distribution of synaptic contacts in single neurons must be addressed in detail. However, it did not examine the impact of the detailed distribution of pre-synaptic contacts in full axon morphologies, and it relies on the underlying assumption that pre-synaptic contacts are uniformly distributed. Complementing these results, a recent article has briefly explored how perturbed dendritic morphology could alter the rat somatosensory minicolumn wiring. The study found that shortening or deleting the dendrites resulted in connection deficits in the neuronal network,[30] which is consistent with observations in neurological disease.[31] However, an exploration of how diverse perturbations in axonal trees and pre-synaptic contact distributions is missing, together with a graph-theoretical detailed analysis of the impact of perturbations on network topology.

The high-throughput generation of single-neuron full morphology reconstructions in the mouse brain offers the possibility of exploring a novel approximation to single-cell whole-brain networks.[32] Subsequent work has provided putative bouton locations throughout the fully reconstructed axonal trees.[33,34] The fact that neurons reconstructed from diverse brains are spatially registered[35] to a common coordinate framework (CCFv3)[36] allows us to analyze axon-dendrite potential connections at the whole-brain level with unprecedented anatomical detail. Although these data are not as precise as electron microscopy quantifications, they provide the advantage of a whole-brain perspective while allowing for the identification of subcellular synaptic structures. Similar to the use of post-synaptic dendritic spines to quantify and describe excitatory input connectivity to dendritic trees, we use axonal boutons as a first approximation to study pre-synaptic connectivity. In fact, axonal boutons have been shown to be a proxy of structural neuronal connectivity.[37] However, reconstructing the full morphology of axonal projections and measuring the locations of single boutons in the context of the complete axonal tree was not possible until recently. For this reason, Peters' rule,[38] a common approximation for quantifying neuronal connectivity at the cellular scale, has been used in the field of computational neuroscience. This rule assumes that there is a potential connection between a nearby axon and a dendrite, implying that synaptic connections are evenly distributed over the axonal and dendritic segments. However, it has been suggested that ground-truth synaptic connectivity follows a nuanced Peters' rule instead.[27] From this perspective, the spatial distribution of pre- and post-synaptic sites and synaptic contact probabilities vary among diverse neuron types, finely tuning network connectivity.

We hypothesize that neuron morphology details determine network wiring. Specifically, we consider that distribution of axonal boutons throughout the axonal tree is not uniform and that such distribution determines network topology. Meanwhile, perturbation of specific morphological properties (i.e., neuron tree size, complexity, and density of axonal boutons) has a differential significant impact on network structure. To test this hypothesis, we devised an algorithm to generate single-cell networks in the whole brain using putative bouton locations and also simulated uniformly distributed boutons throughout the axon. First, we illustrate the biological relevance of axonal bouton distributions. With the networks we generated, we perform a detailed graph-theoretical analysis of the network structure and its dependence on axonal bouton distribution. To contextualize this information and explore its relevance in comparison to biologically plausible neural morphological alterations, we explored the impact of perturbing specific morphological features.

RESULTS

Axonal bouton distribution is cell-type dependent

We analyzed putative axonal bouton locations obtained by another team[34] through automated detection of increased radius and intensity blobs in fully traced axons from neurons with somas located mainly in the thalamic and cortical regions. See the supporting datasets in the data and code availability section for a summary of the number of neurons ($n > 20$) in each analyzed CCFv3 brain region. The spatial distribution of the boutons is mainly determined by the axonal projection pattern of each cell type (Figures 1A and 1B). To explore the biological relevance of the bouton distributions along the axons, we explored them in neurons with similar morphology and soma location in the brain (Figure 1C, top). To identify morphologically similar neurons, we used the topological morphology descriptor (TMD), a method to encode the spatial structure of trees combining morphology and topology.[30,39] The default TMD definition by Kanari et al. defines the barcode of a tree as the set of radial distances to the soma in the birth and death nodes of each branch of the tree. By measuring the distance between barcodes, we obtained pairwise distances between all neurons in each brain region. To quantify the similarity in axon bouton distributions, we defined TMD bouton barcodes as the set of numbers of putative boutons enclosed within spheres with radii defined by the birth and death nodes of each branch of the tree. This reflects a trend in the distribution of putative boutons throughout the tree

of the direct distance, which can also be seen as bouton density. Statistically significant differences between uniform and observed bouton distributions are indicated with a gray shadow; paired-samples t test random vs. observed bouton number per neuron $p < 0.005$, $N_{VPM} = 379$, $N_{SSp\text{-}m} = 78$, $N_{CP} = 325$.
(E) Bar plot of the fitted average bouton density (see STAR Methods) for all neurons in each of the brain regions with more than 20 neurons. Pairwise t tests between brain areas; ***$p < 0.001$. N is the number of neurons in each brain region, indicated in the x axis.

branch (see Figure S1 for a visual). As expected, default TMD and bouton TMD distances are correlated (Pearson correlation coefficient of 0.595 for default TMD vs. bouton TMD distances, N_{neuron_pairs} = 15,549,66). However, TMD distances obtained with measured putative boutons have lower correlation coefficients with default TMD than compared to the case of random bouton locations, indicating that putative bouton locations are biologically meaningful (0.595 vs. 0.829; Figure 1C). As an example, default TMD (Figure S1B, left) has a distribution that is approximately a scaled version of random bouton TMD (Figure S1B, right), which differs from the putative bouton TMD (Figure S1B, middle). Another observation that supports the validity of the data is that bouton density in somatosensory areas (obtained as the total length of axon [14,740,853.79 μm] divided by the number of boutons [1,147,532] in these CCFv3 regions) is 0.0778 boutons per μm, which is close to 0.061 boutons per μm as experimentally measured in adult mice using serial-section electron microscopy data.[37]

To explore whether bouton distributions are non-uniform, we defined null uniform distributions of bouton locations for each neuron (see STAR Methods). Interestingly, the null distribution showed a higher correlation with default TMD than the measured distribution of putative boutons (Figures 1C, bottom, and S2A; Pearson correlation coefficients of 0.829 vs. 0.595 for random and measured, respectively; one-way ANCOVA $F(1, 3{,}109{,}929) = 0.022$, $p = 7.17e{-9}$). This is explained by the fact that our bouton TMD definition is highly sensitive to differences in the total numbers of boutons of morphologically similar neurons (Figure S2B). Correlations between TMD distances segregated for neurons with their somas in specific brain regions show analogous results (Figure S2C). A Sholl analysis of axon length, branch points, and density of boutons showed (see STAR Methods) that putative bouton distributions significantly differ from a uniform distribution (Figure 1D; paired-samples t test random vs. putative bouton number $p < 0.005$). When calculating boutons, we use the path distance to the soma instead of the direct distance, which is also the bouton density through the whole neuron structure. Specifically, the boutons of neurons in the thalamus (ventral posteromedial [VPM]) are preferentially located at the distal axon and have low bouton density near the soma. Neurons in the striatum (caudoputamen [CP]) share similar trends. Conversely, neurons in the somatosensory cortex (mouth primary somatosensory [SSp-m]) show a distribution of boutons that is close to uniform for both proximal and distal axonal branches and significantly lower than uniform in the middle section (see other cell types in Figures S2D and S3A).

Obtaining small fragments of axons and quantifying axonal bouton density is a common practice in electron microscopy studies.[37,40,41] Our results indicate that those estimates may vary among distal and proximal axonal trees. This phenomenon has also been found in studies of substantia nigra reticular part (SNr) neuronal projection areas.[42] To provide improved estimates based on our detailed data, we fitted a uniformly distributed bouton curve to the observed distribution of putative boutons (see STAR Methods). Neurons with their somas in different brain regions showed different average bouton density values (Figure 1E; paired samples t test cortex vs. thalamus $p < 2e{-16}$, cortex vs. striatum $p < 2e{-16}$, cortex vs. hippocampus $p = 0.98$, hippocampus vs. thalamus $p = 1.1e{-9}$, hippocampus vs. striatum $p = 9.2e{-5}$, striatum vs. thalamus $p = 3.9e{-11}$). The average bouton density of the analyzed cell types ranged from 0.029 to 0.104 boutons per μm.

As previously described for neocortical inhibitory neurons,[43] we found that lower Strahler order[44,45] segments (tip or close-to-tip segments) have the highest density of boutons, decreasing toward higher Strahler order segments, especially above 2 (Figure S3B). Interestingly, the Strahler order distribution of bouton densities varied among neurons with somas in different brain regions (Figure 1F; all pairwise t tests $p < 0.05$ except for SSp-m vs. VPM in Strahler orders 3 and 4). The low variance in the bouton density within each Strahler order indicates that those can be considered homogeneous.

Generation of connectivity matrices based on full neuron reconstructions

To investigate the details of single-cell morphology, including the size and complexity of axons and dendrites, and the specific effects of the number and distribution of boutons on the network, we devised a method for constructing single-cell networks based on full neuron tracings. We argue that if there are axon boutons and dendrites in close spatial proximity, then they have a high probability of producing synaptic contact.[27] To generate connectivity matrices, we divided the whole brain into 30 × 30 μm cubes (see STAR Methods) and measured the axon length, dendrite length, and bouton number of each neuron within each cube (Figure 2A). We consider that when both axons and dendrites are present in a cube containing boutons, there is a potential connection (Figure 2B). Then, we defined the connection strength (Figure 2C) as follows. Considering that an axon may connect to many dendrites in the same cubic volume, we set the strength of the connection proportional to the number of boutons and to the proportion of the length of each dendritic tree. Specifically, the connection strength of the pre-synaptic neuron n with the post-synaptic neuron m in a single cube is defined as

$$C^k_{nm} = N\_b^k_n * P\_d^k_m \qquad \text{(Equation 1)}$$

In cube k, the number of boutons of neuron n is $N\_b^k_n$ and the proportion of dendrite length of neuron m is $P\_d^k_m$, meaning the length of the dendrite of neuron m in cube k over the total length of all dendrites having connections in cube k (see STAR Methods). The multiplication of the two provides the connection strengths of neuron n and neuron m in cube k, which is C^k_{nm}. It is important to note that dendrite length is used here to distribute the existing pre-synaptic contacts among different post-synaptic neurons occupying the same cube. We obtained the full-brain single-cell connectivity matrix by adding the results obtained on all cubes covering the mouse brain in CCFv3 (Figure 2D).

We applied this network generation method to our single-cell data with observed bouton locations (observed network). To explore the relevance of the bouton distribution on the network topology, we also generated a uniform network, setting boutons throughout the axon using the average bouton density for each cell type we obtained previously (Figure 1E).

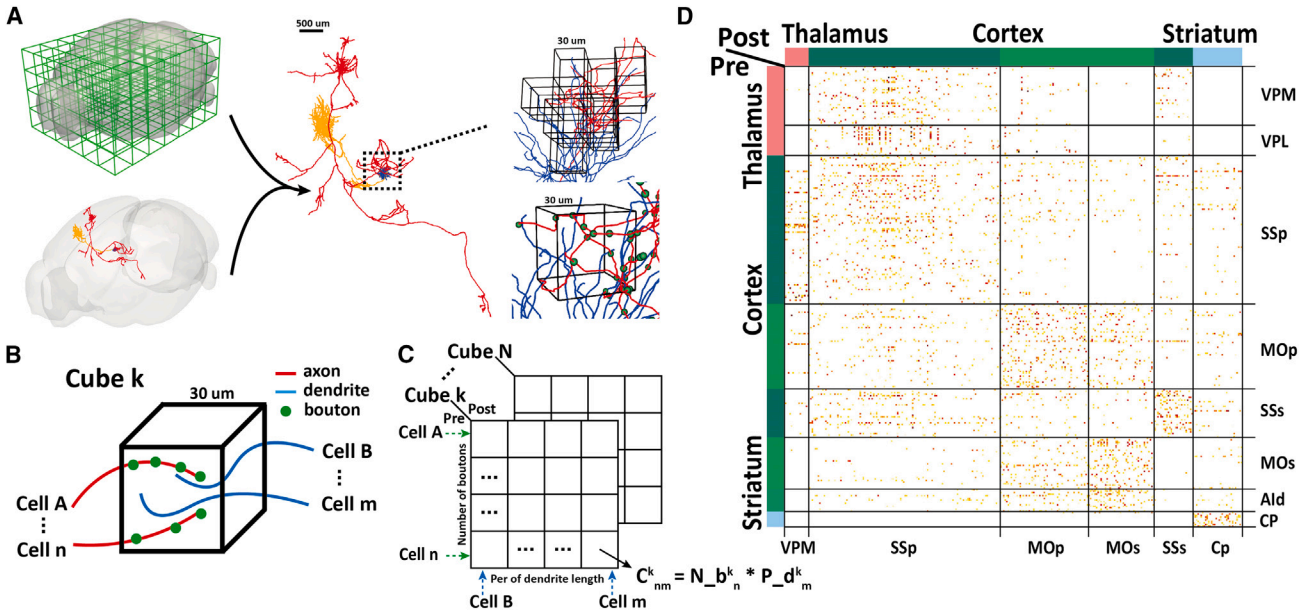

Figure 2. Generation of connectivity matrices based on full neuron reconstructions

(A) 3D rendering of the division of the whole brain into cubes of 30 μm units (top left) and full neuron reconstruction registered to CCFv3 (bottom left). Close-up rendering of a pair of neurons (dendrites in blue and axons in red and orange; middle). Rendering of a region of interest where axons and dendrites are close by in CCFv3 space (top right) and where the length of dendrite and the number of axonal boutons (green dots) can be obtained within each cube (bottom right).

(B) Schematic visualization of the coexistence of axon and dendrite within each cube, which define connectivity together with axonal boutons.

(C) Schematic visualization of our procedure to obtain the connection strength between each pair of neurons in a cube according to the number of boutons and the dendrite length of each post-synaptic neuron found in the cube.

(D) Visualization of a subset (304 and 306 pre- and post-synaptic neurons, respectively) of the whole-brain single-cell connectivity matrix.

Bouton distribution tunes network topology and influences community structure

A comparison between our observed connectivity matrix and the mesoscale connectome obtained previously with tracer injections[24] shows similar connectivity clusters (Figure S3C), suggesting that even though our single-neuron data account for a very small percentage of the network, they can recapitulate the mesoscopic structure. The uniform network shows a bias toward increased connectivity, with 1,847 nodes and 22,882 edges compared to the observed network with 1,781 nodes and 14,056 edges. The small difference in the number of nodes is due to the removal of neurons with 0 potential connections. Circular plots of the network structure show that there are a large number of potential connections between the cortex, thalamus, and striatum, as well as local potential connectivity (Figure 3A).

To explore the community structure, we used the Leiden community detection algorithm[46] (see STAR Methods) on the two networks. Remarkably, the circular plots show that the bouton distribution tunes the community structure in the network. We assessed the number of neurons in each community and found that, in the observed network, the largest community of neurons (N = 206) belongs to the thalamo-cortical loop in the left hemisphere (mainly from VPM to SSp barrel field [SSp-bfd] in the cortex; Figures 3A and S4A). However, this loop is under-represented in proportion in the uniform network, being the third largest community (N = 215) (Figure S4B). The second largest community in the observed network (N = 179) is defined by the right hemisphere thalamo-cortical loop with a higher representation of the ventral posterolateral nucleus of the thalamus (VPL) and medial geniculate complex (MG) in the thalamus and other cortical areas such as the supplemental somato-sensory area (SSs) and the retrosplenial area, ventral part (RSPv). The most similar community in the uniform network is larger in proportion (N = 256), having an over-representation of primary visual area (VISp) neurons. The third largest community in the observed network is the cortex-thalamus-striatum loop of cortical neurons with CP and VPM (N = 172). This community is the second largest in the uniform network (N = 234), where the motor cortex, CP, and the agranular insular area dorsal part (AId) are over-represented. Conversely, for this community, SSp neurons are under-represented in the uniform network.

Previous studies show that there are some simple organizational patterns such as the degree distributions[47] in brain networks that can be explained using network models.[3] To explore this, we generated three artificial networks, random, small world, and scale-free, with the same number of nodes and edges as the observed network for comparison. Given that Oh et al.[24] showed that the mouse brain network has small-world topology traits (namely large clustering coefficient and short average path length[48]), we tested whether the observed and uniform networks follow this trend. In the random network, the average path length is 3.852, and the clustering coefficient is 8.96e−3, compared to the observed average path length of 4.828 (uniform: 4.257) and clustering coefficient of 0.184 (uniform: 0.195) in the observed network (supporting datasets can be found in the data and code availability section). These results are consistent with

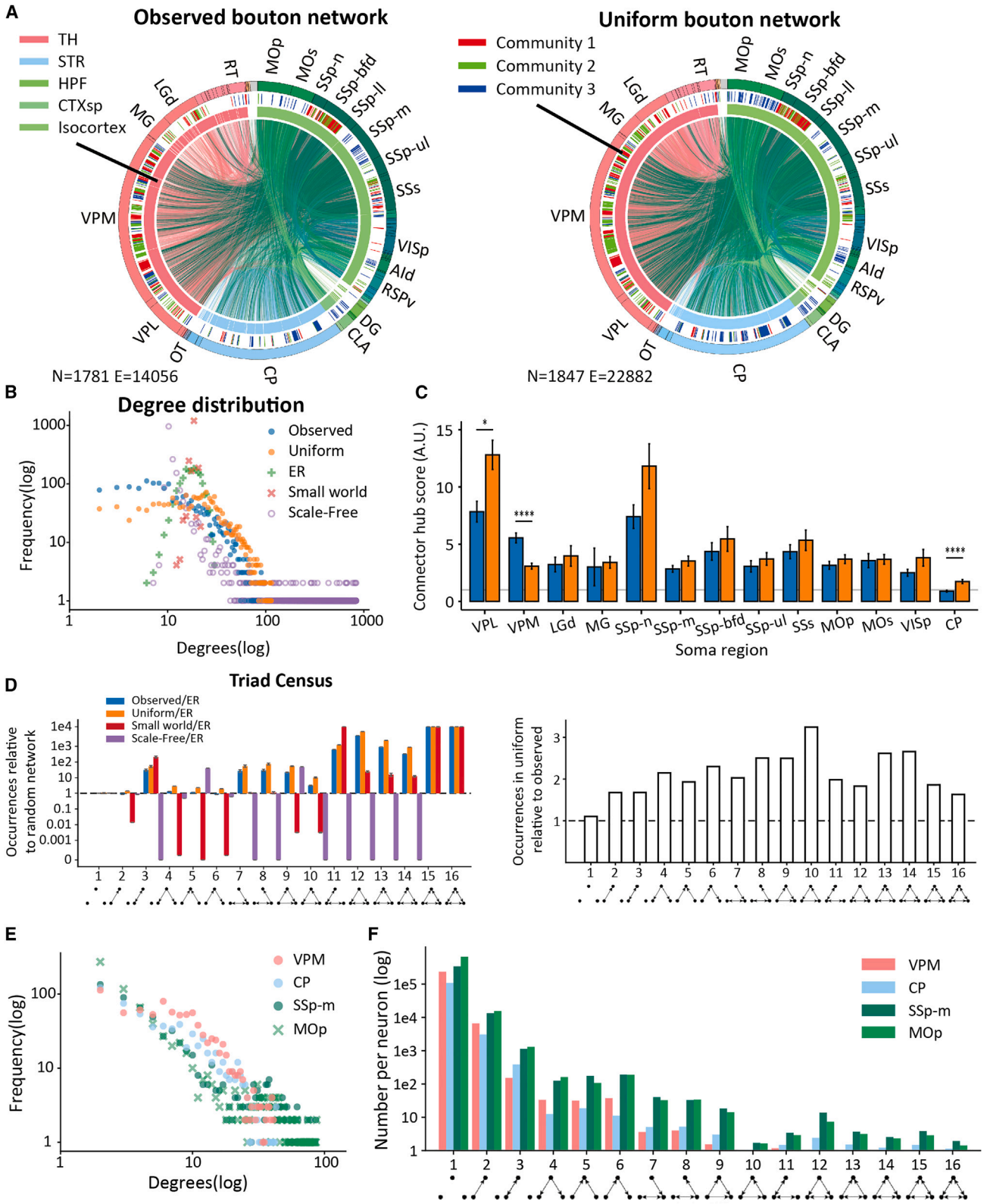

(legend on next page)

previous data.[24] However, the model that best approximates the degree distribution of the observed and uniform networks is the scale-free network (Figure 3B; Spearman correlation observed vs. scale-free $r(1,779) = 0.242$, $p < 0.001$; observed vs. random network $r(1,779) = 0.029$, $p > 0.1$; observed vs. small-world network $r(1,779) = 0.0136$, $p > 0.1$, N is the number of edges in different networks). However, degree distributions strongly differ among all cases (see supporting datasets in the data and code availability section for pairwise two-sample Kolmogorov-Smirnov tests; $p < 1e{-}83$). When comparing observed with uniform, the degree distribution shows an increased proportion of high-degree nodes (two sample Kolmogorov-Smirnov $D(1,779) = 0.297$, $p < 0.001$).

To better understand this difference, we tested whether high-degree nodes are different among the two networks. We obtained hub and authority scores for anatomically defined brain regions.[49] The brain regions with the highest hub scores are SSp-m and VPM in both networks (supporting datasets can be found in the data and code availability section). Authority nodes are mainly cortical regions (including nose SSp [SSp-n], SSs, SSp unassigned [SSp-un], SSp-m, and SSp-bdf) for the observed network but also include CP, VPL, and VPM in the uniform network. This reflects neural sinks and sources in hub regions.[25] Also, these hubs are consistent with global functional hubs and high connection diversity hubs in mouse functional networks.[50] Those can be linked to the integration and segregation of the networks[51] by measuring the ratio between local and inter-region potential connections, which identify provincial and connector hubs. We found that the uniform network tends to have higher connector hub scores except for VPM (Figure 3C; pairwise t test observed vs. uniform VPL $p = 0.017$, VPM $p = 8.1e{-}7$, and CP $p = 1.3e{-}5$, N is the number of neurons in each brain region: $N_{VPL} = 80$, $N_{VPM} = 379$, and $N_{CP} = 325$). This also suggests that the specific distribution of axonal boutons can have functional implications and is relevant to understand the contribution of each brain region in information transmission and processing throughout the brain.

The pattern of potential connections between triads is the most basic motif forming the networks,[52] and its distribution reflects the rules of neuronal connectivity.[29] We found that observed and uniform networks have similar triad distributions (Figure S4C; two-sample Kolmogorov-Smirnov $D(14) = 0.3125$, $p = 0.42$), and both strongly differ from random, small-world, and scale-free networks (Figure 3D, top; supporting datasets in the data and code availability section), showing more prominent feedback and complex potential connections compared to the expected occurrence in random networks (Figure 3D; supporting datasets in the data and code availability section). This result is consistent with previous observation in cortical microcircuits, but we noticed more complex motifs between three neurons in networks, which were missing in previous studies. We assume this is because our data have an unprecedented level of detail and a number of reconstructions.[29,53,54] Meanwhile, the uniform network overestimates all network motifs in comparison to observed, with an average ratio of 2.1 (Figure 3D, right), highlighting a methodological artifact in studies assuming homogeneous axonal bouton distributions.

We analyzed the subnetworks composed of established anatomical types of neurons within thalamus (VPM), striatum (CP), and cortex (SSp-m and primary motor area [MOp]). VPM neurons receive input from the cortex and project to the cortex and thalamus (Figure S5A). CP neurons receive inputs primarily from the cortex and a few from the thalamus, with many local connections. SSp-m and MOp neurons both receive inputs from the thalamus and striatum (mainly CP) and interconnect with other cortical layers (Figure S5B, left). MOp has more connections to the lower limb somatosensory cortex (SSp-ll) and secondary motor areas (MOs) compared to SSp-m. All subnetworks showed similar trends in terms of degree distribution and triads compared to random and scale-free networks (Figure S5B, middle). Interestingly, neurons in the cortex (SSp-m, MOp) have more high-degree nodes compared to neurons in the thalamus and striatum (VPM, CP) (Figures 3F, S5C, and S5D). The motif distribution of VPM neurons mainly contained low-complexity motifs communicating between pairs of neurons or one direction transmission among three neurons. However, the distribution for CP, SSp-m, and SSs neurons showed more high-complexity motifs with multi-directional three-neuron intercommunications (Figure 3F). This is consistent with the knowledge of the thalamus as an anatomically critical node for transmitting information.[55] In this line, we also attempted to examine the subnetworks of neurons in cortical layers (layer 2/3 and layer 5, limited to those to ensure enough neurons for the analysis). The nodes in both subnetworks all have high

Figure 3. Bouton distribution tunes network topology and influences community structure

(A) Circular plot visualization of the single-cell networks constructed based on observed (left) and uniform (right) bouton data. We assigned the colors in the outer circle by the soma location of each neuron in the network. The middle circle indicates the largest three communities obtained using the Leiden algorithm,[46] and the inner circle indicates the broad brain regions TH, STR, hippocampal formation (HPF), cortical subplate (CTXsp), and isocortex. The lines crossing the center of the circle indicate potential connections between individual neurons. We colored them according to the soma location of the pre-synaptic neuron.

(B) Scatterplot of the degree distributions of observed (blue), uniform (orange), Erdös-Rényi (ER; green), small-world (red), and scale-free (purple) networks.

(C) Bar plot of connector hub scores for the soma regions with at least 50 neurons for observed (blue) and uniform (orange) networks. The gray line indicates connector hub score 1, which indicates the same proportion of edges within and across regions. Pairwise t test *$p < 0.05$ and ****$p < 0.0001$, N is the number of neurons in each brain region. Bars indicate mean values ± standard error of the mean.

(D) Bar plot of triad occurrence is relative to endoplasmic reticulum (ER) networks with the same number of nodes and edges (left) of observed (blue), uniform (orange), small-world (red), and scale-free (purple) networks. Bars indicate mean values ± standard deviation. Bar plot of triad occurrence in the uniform network relative to observed (right). The dashed lines indicate no difference (ratio = 1). The bottom row shows schematic visualizations of the network motifs identified with each index from simple to complex.

(E) Scatterplot of the degree distribution of different subnetwork based on cell types. We chose the type in TH (VPM, pink), STR (CP, blue), and cortex (SSp-m, green node; MOp, green cross).

(F) Bar plot of triad occurrence in different subnetworks based on cell types. We calculated the number of triad occurrences for each neuron.

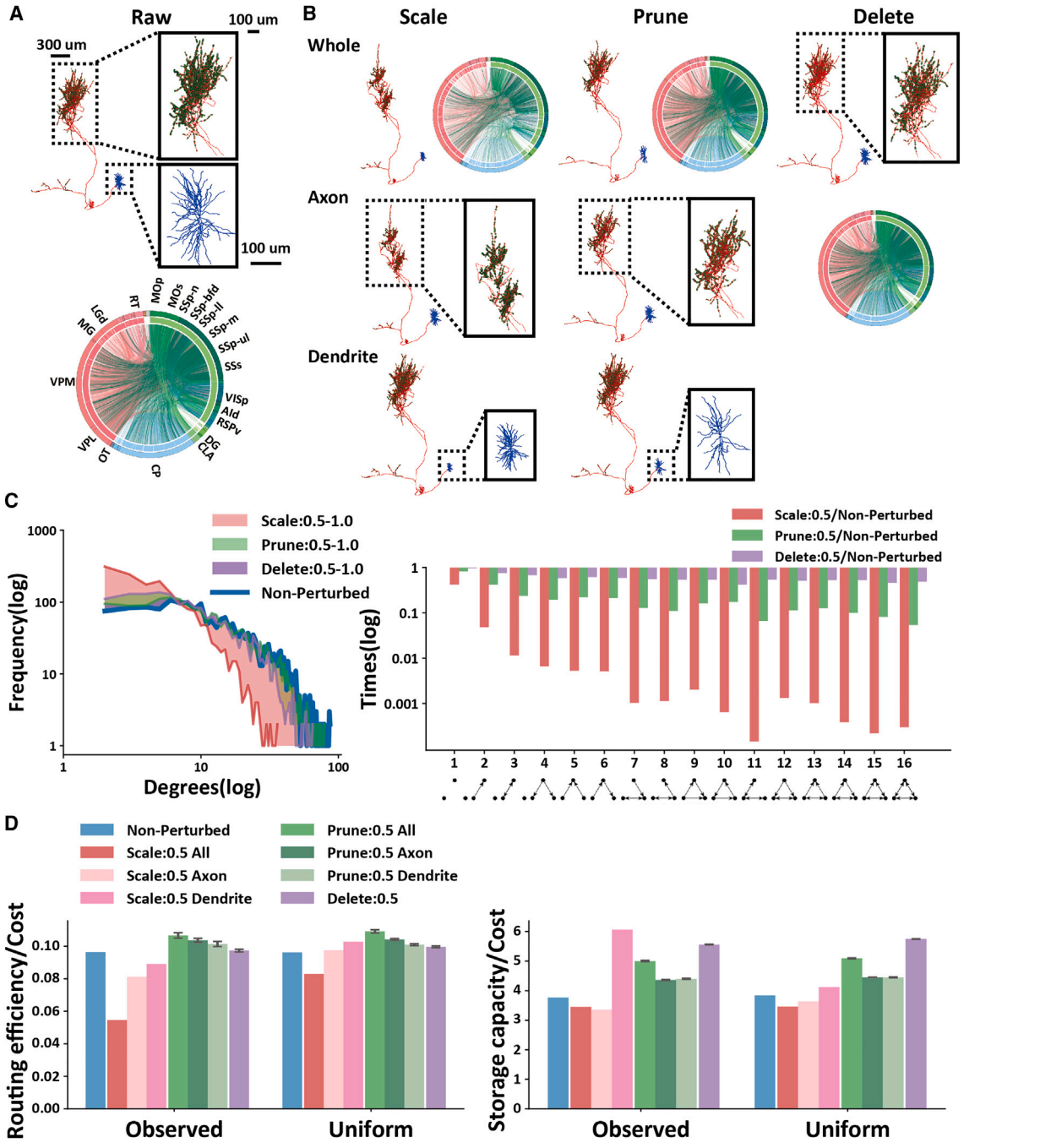

Figure 4. Dendritic and axonal tree spans are the main determinants of network topology

(A) Representative example of a full morphology neuron (top) with magnifications of dendritic (blue) and axonal (red) arbors. The axonal arbor magnification shows axonal boutons as green dots. The circular plot of the observed unperturbed network (bottom). Colors in the outer circle indicate the soma location of each neuron. The inner circle indicates the broad brain regions TH, STR, HPF, CTXsp, and isocortex. The lines crossing the center of the circle indicate potential connections between individual neurons, colored according to the soma location of the pre-synaptic neuron.

(B) Representative visualizations of single-neuron perturbations in both dendritic and axonal arbors of the neurons (top row), only in axonal arbors (middle row), and only in dendritic arbors (bottom row). The perturbations include scaling of the tree span (left row), pruning of branches (middle column), and deletion of boutons (right column). Scale bars: 100 μm.

(C) Line plot of the degree distributions (top) for the unperturbed observed network (blue) and for scale (orange), prune (green), and bouton deletion (purple) perturbations in both dendritic and axonal arbors. The colored shadows indicate the range in which degree distributions vary with each perturbation with ratios

(legend continued on next page)

degrees and contain complex connectivity patterns. Due to data limitations, we do not see a difference between the two layer 5 neurons that tend to have higher degree connectivity and tend to form more complex motifs (Figure S5F). However, those results should be interpreted carefully given the limitations in spatial registration to CCF (see limitations of the study).

Overall, our results suggest that the detailed distribution of axonal boutons is a relevant determinant of the network topology. Taking into account that the basic function of brain networks is to transfer and store information, we measured cost (defined as the total number of boutons in the network), routing efficiency,[56] and storage capacity,[57] which are topological correlates of the network functional performance[58] (see STAR Methods). Since the uniform network has more edges and stronger potential connections, its cost, routing efficiency, and storage capacity are 1.563, 1.561, and 1.595 times higher than the observed network, respectively (Figure S4D). But the average routing efficiency and storage capacity per bouton, which is the value divided by cost and is representative of the Pareto optimality of the network,[58] did not change (normalized routing efficiency and storage capacity are 9.6e−3 and 0.38 a.u., respectively, for both networks). Thus, it remains an open question whether non-random distributions of axonal boutons imply any functional advantage from an energy optimization perspective.

Dendritic and axonal tree spans are the main determinants of network topology

To analyze the impact of putative morphological alterations relevant to cognitive impairments,[59–64] we perturbed the networks as follows: scaling neuron size, pruning neuron branches, and removing axonal boutons (see STAR Methods). Tree span has the greatest impact on the network, implying a marked shift toward lower-degree potential connections (Figures 4C, left, and S6A; Kolmogorov-Smirnov unperturbed vs. scale all 0.5 $D(86) = 0.477$, $p = 6.5e{-9}$, N is the number of degrees) and orders of magnitude lower occurrence of complex network motifs (Figure 4C, right; Kolmogorov-Smirnov unperturbed vs. scale all 0.5 $D(14) = 0.438$, $p = 0.0933$, N is the kind of triad motifs). Conversely, pruning and bouton deletion, even when reducing the number of branches or boutons to half, had a modest impact on degree distribution (Figure 4C, left; Kolmogorov-Smirnov unperturbed vs. prune all 0.5 $D(86) = 0.198$, $p = 0.07$; Kolmogorov-Smirnov unperturbed vs. bouton delete all 0.5 $D(86) = 0.093$, $p = 0.85$, N is the number of degrees) and the triad census (Figure 4C, right; Kolmogorov-Smirnov unperturbed vs. prune all 0.5 $D(14) = 0.25$, $p = 0.716$; Kolmogorov-Smirnov unperturbed vs. bouton delete all 0.5 $D(14) = 0.125$, $p = 0.999$, N is the kind of triad motifs).

Similarly, we investigated the community structure of different networks after perturbation. Pruning of axonal and dendritic branches, or bouton removal, does not imply marked differences in the community structure (Figures S7A–S7C). The top two communities are still the cortico-thalamic loop of both hemispheres and the third is a cortico-thalamic-striatal loop. However, the scaling of dendritic and axonal trees sharply reduced the number of potential connections (having 3,955 edges compared to 14,056 in the observed network), strongly impacting the community structure (Figure S7D). While dendritic scaling strongly reduced the number of potential connections (average of 373 potential connections per community) in comparison to axonal scaling (average of 760 potential connections per community), the change in the community structure for axonal scaling implied losing the thalamic connection in the thalamo-cortical-striatal circuit (Figure S7C).

When we measured routing efficiency in the networks perturbed with pruning and bouton deletion, we found that the reduction in routing efficiency provoked by the perturbations is compensated by the reduction in cost (Figure 4D, left; absolute value in Figure S6B). Interestingly, the impact of both axonal and dendritic tree downscaling implied a marked reduction (43.35%) of the routing efficiency per unit of cost in the observed network but had only a subtle impact (13.74%) in the uniform network (Figure 4D, left; Figure S6C). This indicates that the impact of tree span perturbations may be underestimated in generative models not taking into account precise pre-synaptic connection distributions in the axon. Morphological perturbations showed a subtle increase in storage capacity per unit of cost (Figures 4D, right, and S6C). This is explained by the fact that the approximation we used for storage capacity is mainly dependent on the combinatorics of diverse afferents on the same post-synaptic neurons.[57] Interestingly, the observed network showed a storage capacity per unit of cost markedly higher than in the uniform network (60.99%) when only dendritic trees are downscaled (Figure 4D, right). This is the only case in which the observed distribution of putative boutons appears to have a strong impact on network topology. This result suggests that the synaptic targeting of diverse axonal arbors is precisely matched with post-synaptic dendrites, implying that even when strongly reducing dendritic tree size, post-synaptic neurons can still keep receiving inputs from a diverse set of incoming axons.

To assess the robustness of our results considering that the experimental data are highly sparse, we removed half of the neurons in the observed network (Figure S8A). We found that both the degree distribution and triad census did not vary in comparison to the observed network (Figures S8B and S8D), while the community structure and routing efficiency and the storage capacity per unit of cost markedly increased (by factors of 2.02 and 1.71, respectively; Figure S8C). This suggests that increasing the numbers of neurons used to generate whole-brain connectivity networks is necessary to accurately assess circuit architecture.

DISCUSSION

Many datasets and analyses of the detailed morphology of full neurons have become available recently.[32,65,66] However, those do not describe in detail the impact of axonal branching on potential connectivity. From the single-cell perspective, at a more

between 0.5 and 1. Bar plot (bottom) of triad occurrence relative to the observed unperturbed network for scale (orange), prune (green), and bouton deletion (purple) perturbations. The bottom row shows schematic visualizations of the network motifs identified with each index from simple to complex.
(D) Bar plots of routing efficiency (left) and storage capacity (right) divided by the cost (number of potential contacts) for the unperturbed observed and uniform networks (blue) and after scale (red), prune (green), and bouton deletion (purple) perturbations. Bars indicate mean values ± standard deviation.

local level, previous work from our lab addressed the subcellular organization of post-synaptic sites in cortical layer 2/3 pyramidal cells. We showed that the precise distribution and balance of excitatory and inhibitory synapses shape single-neuron firing.[2] Quantifying the precise distribution of pre-synaptic contacts in full axons of mammal neurons has been addressed in some studies that require arduous manual effort for their annotation.[37,40,41,67] In this work, we leverage automatically identified putative axonal bouton locations obtained by our team.[34] In accordance with previous studies, our analysis shows that pre-synaptic contact locations are not homogeneous throughout the axon[68,69] and that they vary among brain regions.[41,42,70] However, these previous works focused on spatial averages of bouton density, without addressing cell-to-cell connectivity.[42] Another limitation of previous works is they focus on small numbers of neurons in very specific neural types.[41] In this work, we quantify bouton distributions in 1,891 single neurons from 97 brain regions. While previous approximations are consistent with an enrichment of boutons in projection areas, our data provide the most accurate and complete description of non-homogeneous bouton distribution throughout axonal trees to date. The consistency we found in morphologically similar neurons suggests that the putative bouton connection data we used are sufficient as a first approximation. Similarly, the low variance we found in our quantification of increased axonal bouton density in terminal branches is supported by previous evidence in local axonal trees, which has been suggested to enhance temporal economy and precision in neocortical inhibitory axonal trees.[43] The fact that this phenomenon is found for all the neurons we analyzed indicates that it is a fundamental principle determining pre-synaptic contact distribution. We expect that those neuron morphological properties will have relevant physiological implications. From the dendritic perspective, it is well known that branching patterns have strong impacts on single-neuron firing and computation that permeate to impact network activity and behavioral performance in cognitive tasks.[71–73] It is reasonable to expect that such morphological features will also be relevant in the physiology of axonal trees. Still, further refining the methods to consider multiple synapses in single boutons and pre-synaptic sites in the absence of boutons will be necessary in the future. Those can be constrained reliably based on electron microscopy observations of specific cell types. However, electron microscopy quantifications in isolated neuropile blocks or small neurite fragments are not sufficient to approximate network connectivity.[27] By combining such quantifications with whole-brain neuronal morphometry in a cell-type-based manner, we can leverage the advantages of both techniques to describe neuronal circuitry with increased throughput.[71–73]

One relevant aspect of our work is its special focus on long-range projections, together with the development of the method to generate whole-brain single-cell connectivity matrices. It is worth noting that the aim of this work is not to generate accurate and complete connectivity matrices but to explore the relevance of non-homogeneous pre-synaptic contact distributions on the network structure. Our algorithm for the generation of connectivity matrices based on full morphology neuronal reconstructions is open source, and our scripts conform to a pipeline to generate full-brain networks with datasets that are expected to grow exponentially in the future. Our comparison between observed and uniform bouton distributions and their impact on network structure supports the claim that Peters' rule is an over-simplified model, which cannot truly reflect the differences in connections between brain regions and between neurons. It overestimates the possibility of the existence of connections, which leads to an overall bias in the properties of the network and significant differences in its community structure and provincial vs. connector hub scores, which is relevant for functional integration and segregation.[3] These results are consistent with previous findings in the cortical network architecture, where most overlapping axons and dendrites are not connected, and the more dendrites from different neurons the axon is exposed to, the less probability there is that a connection exists.[29]

The network properties we found in single-cell networks also complement our understanding of neuronal wiring rules. The observed bouton network we analyzed shows increased occurrence of feedback and complex network motifs than what would be expected in random networks, which is consistent with the result found in the barrel cortex.[29] Our results indicate that such a pattern in the distribution of network motifs is not unique to cortical networks but is also present in the thalamo-cortical loop. Also in this study, the network was found to have small-world properties, which was also confirmed in our single-cell network. The degree distribution is close to scale free, and the clustering coefficient is small.[24]

Existing studies suggest that neurological diseases such as intellectual disability, autism spectrum disorder, epilepsy, schizophrenia, and bipolar disorder are accompanied by a decrease in dendrite branches and spines with atrophy of the dendrite morphology.[1,59,60,62,63] The most influential of these changes is the decrease in the spine and the change in morphology.[31] Deformation and damage of axons can also lead to various neurological diseases.[61,64] This phenomenon can be seen in our perturbations. The biggest impact on the network properties is the dendritic and axonal tree span scaling. And the studied network is more robust to bouton removal and pruning of branches, which is also supported by previous literature.[74] All operations on dendrites have a greater impact than on axons for degree and network motif distributions. However, it is interesting to note that dendrite downscaling shows increased storage capacity per number of connections for the observed network, while the same quantity does not change for the uniform network. This is an unexpected result suggesting that the precise location of axonal boutons in diverse axonal arbors allows us to keep high input combinatorics in single dendritic trees even with marked downscaling of the dendritic span.

Limitations of the study

It is important to note that we do not aim to provide an accurate synaptic scale connectome description in this paper but rather a first approximation for whole-brain network architecture based on full neuron tracings and bouton location data. Because of the limited neuron and bouton data, the connectivity is very sparse on a whole-brain scale. Thus, the total number of putative detected boutons was 3,825,227, of which 181,691 (4.7%) were identified as having potential connections with dendrites in our

dataset. Moreover, there is a bias in the number of neurons on cell type. Only three types of neurons, VPM (385), CP (325), and SSp (253), had numbers above 100, and these three cell types accounted for one-half of the total data (1,891). This leads to a specific description of the thalamo-cortical-striatal circuit. It is reasonable to expect that the observations reported here may differ when more data become available. However, we are confident that the main features and trends we report provide valuable information toward the analysis and simulation of whole-brain circuits at the single-neuron level.

The great variation in the size of the original brain leads to some stretching and shifting of the neuron in the registration. Some of the neurons, especially the neurons near the surface of the cortex, had some axons beyond the atlas volume. According to our statistics, there are 738 neurons with data points beyond the CCFv3 boundary. Among these neurons, the number of out-of-bounds points is 7.46% of all points. This is also one of the reasons we chose the cube size of 30 μm. There is no better registration solution currently unless mass manual proofreading is used. Still, soma locations all lay within the atlas volume, and our connectivity generation method only requires axon and dendrite colocalization, regardless of their location in space.

We did not aim to link our connectivity patterns exploration with specific anatomical circuit descriptions here. While this is a limitation of the current manuscript, ongoing studies from our team are addressing those in detail.[75]

STAR★METHODS

Detailed methods are provided in the online version of this paper and include the following:

- KEY RESOURCES TABLE
- RESOURCE AVAILABILITY
  - Lead contact
  - Materials availability
  - Data and code availability
- METHOD DETAILS
  - Sources of experimental data
  - Calculation of bouton distribution
  - Generation of networks
  - Network analysis
  - Community detection
  - Multi-objective optimality metrics
  - Cost
  - Storage capacity
  - Routing efficiency
  - Perturbation
  - Scaling of neuron size
  - Pruning of neurites
  - Removal of boutons
- QUANTIFICATION AND STATISTICAL ANALYSIS

SUPPLEMENTAL INFORMATION

Supplemental information can be found online at https://doi.org/10.1016/j.celrep.2024.113871.

ACKNOWLEDGMENTS

We thank Zhixi Yun, Feng Xiong, and Lijun Wang for comments on the figures. This work was mainly supported by a Southeast University (SEU) initiative of neuroscience awarded to H.P. H.P. was also supported by a Zhejiang Lab BioBit Program visiting grant (2022BCF07).

AUTHOR CONTRIBUTIONS

H.P. and L.M.-G. conceived and designed the study. S.J. generated and provided the full morphology bouton data. P.Q. and L.M.-G. achieved all analysis results and wrote the paper with help from all authors.

DECLARATION OF INTERESTS

The authors declare no competing interests.

Received: September 9, 2023
Revised: January 8, 2024
Accepted: February 9, 2024

REFERENCES

1. Kulkarni, V.A., and Firestein, B.L. (2012). The dendritic tree and brain disorders. Mol. Cell. Neurosci. *50*, 10–20.
2. Iascone, D.M., Li, Y., Sümbül, U., Doron, M., Chen, H., Andreu, V., Goudy, F., Blockus, H., Abbott, L.F., Segev, I., et al. (2020). Whole-neuron synaptic mapping reveals spatially precise excitatory/inhibitory balance limiting dendritic and somatic spiking. Neuron *106*, 566–578.e8.
3. Lynn, C.W., and Bassett, D.S. (2019). The physics of brain network structure, function and control. Nat. Rev. Phys. *1*, 318–332.
4. Sherrington, C. (1907). The integrative action of the nervous system. J. Nerv. Ment. Dis. *34*, 801–802.
5. Hilgetag, C.-C., Burns, G.A., O'Neill, M.A., Scannell, J.W., and Young, M.P. (2000). Anatomical connectivity defines the organization of clusters of cortical areas in the macaque and the cat. Philos. Trans. R. Soc. Lond. B Biol. Sci. *355*, 91–110.
6. Parente, F., and Colosimo, A. (2020). Functional connections between and within brain subnetworks under resting-state. Sci. Rep. *10*, 3438.
7. Azulay, A., Itskovits, E., and Zaslaver, A. (2016). The C. elegans connectome consists of homogenous circuits with defined functional roles. PLoS Comput. Biol. *12*, e1005021.
8. Bassett, D.S., Greenfield, D.L., Meyer-Lindenberg, A., Weinberger, D.R., Moore, S.W., and Bullmore, E.T. (2010). Efficient physical embedding of topologically complex information processing networks in brains and computer circuits. PLoS Comput. Biol. *6*, e1000748.
9. Lesicko, A.M.H., Hristova, T.S., Maigler, K.C., and Llano, D.A. (2016). Connectional modularity of top-down and bottom-up multimodal inputs to the lateral cortex of the mouse inferior colliculus. J. Neurosci. *36*, 11037–11050.
10. Sohn, Y., Choi, M.-K., Ahn, Y.-Y., Lee, J., and Jeong, J. (2011). Topological cluster analysis reveals the systemic organization of the Caenorhabditis elegans connectome. PLoS Comput. Biol. *7*, e1001139.
11. Suárez, L.E., Markello, R.D., Betzel, R.F., and Misic, B. (2020). Linking structure and function in macroscale brain networks. Trends Cogn. Sci. *24*, 302–315.
12. Taylor, P.N., Wang, Y., and Kaiser, M. (2017). Within brain area tractography suggests local modularity using high resolution connectomics. Sci. Rep. *7*, 39859.
13. Sporns, O., and Betzel, R.F. (2016). Modular brain networks. Annu. Rev. Psychol. *67*, 613–640.
14. Sporns, O., and Zwi, J.D. (2004). The small world of the cerebral cortex. Neuroinformatics *2*, 145–162.

15. Sporns, O., Tononi, G., and Edelman, G.M. (2000). Theoretical neuroanatomy: relating anatomical and functional connectivity in graphs and cortical connection matrices. Cereb. Cortex *10*, 127–141.

16. Bullmore, E., and Sporns, O. (2012). The economy of brain network organization. Nat. Rev. Neurosci. *13*, 336–349.

17. Liao, X., Vasilakos, A.V., and He, Y. (2017). Small-world human brain networks: perspectives and challenges. Neurosci. Biobehav. Rev. *77*, 286–300.

18. Van den Heuvel, M.P., and Sporns, O. (2013). Network hubs in the human brain. Trends Cogn. Sci. *17*, 683–696.

19. Gong, G., He, Y., Concha, L., Lebel, C., Gross, D.W., Evans, A.C., and Beaulieu, C. (2009). Mapping anatomical connectivity patterns of human cerebral cortex using in vivo diffusion tensor imaging tractography. Cereb. Cortex *19*, 524–536.

20. Sporns, O. (2022). Structure and function of complex brain networks. Dialogues Clin. Neurosci. *15*, 247–262.

21. Deco, G., Tononi, G., Boly, M., and Kringelbach, M.L. (2015). Rethinking segregation and integration: contributions of whole-brain modelling. Nat. Rev. Neurosci. *16*, 430–439.

22. Kaiser, M., and Hilgetag, C.C. (2006). Nonoptimal component placement, but short processing paths, due to long-distance projections in neural systems. PLoS Comput. Biol. *2*, e95.

23. Latora, V., and Marchiori, M. (2001). Efficient behavior of small-world networks. Phys. Rev. Lett. *87*, 198701.

24. Oh, S.W., Harris, J.A., Ng, L., Winslow, B., Cain, N., Mihalas, S., Wang, Q., Lau, C., Kuan, L., Henry, A.M., et al. (2014). A mesoscale connectome of the mouse brain. Nature *508*, 207–214.

25. Coletta, L., Pagani, M., Whitesell, J.D., Harris, J.A., Bernhardt, B., and Gozzi, A. (2020). Network structure of the mouse brain connectome with voxel resolution. Sci. Adv. *6*, eabb7187.

26. Knox, J.E., Harris, K.D., Graddis, N., Whitesell, J.D., Zeng, H., Harris, J.A., Shea-Brown, E., and Mihalas, S. (2019). High-resolution data-driven model of the mouse connectome. Netw. Neurosci. *3*, 217–236.

27. Rees, C.L., Moradi, K., and Ascoli, G.A. (2017). Weighing the evidence in Peters' rule: does neuronal morphology predict connectivity? Trends Neurosci. *40*, 63–71.

28. Rees, C.L., Wheeler, D.W., Hamilton, D.J., White, C.M., Komendantov, A.O., and Ascoli, G.A. (2016). Graph theoretic and motif analyses of the hippocampal neuron type potential connectome. Eneuro *3*, ENEURO.0205-16.2016.

29. Udvary, D., Harth, P., Macke, J.H., Hege, H.-C., de Kock, C.P.J., Sakmann, B., and Oberlaender, M. (2022). The impact of neuron morphology on cortical network architecture. Cell Rep. *39*, 110677.

30. Kanari, L., Dictus, H., Chalimourda, A., Arnaudon, A., Van Geit, W., Coste, B., Shillcock, J., Hess, K., and Markram, H. (2022). Computational synthesis of cortical dendritic morphologies. Cell Rep. *39*, 110586.

31. Forrest, M.P., Parnell, E., and Penzes, P. (2018). Dendritic structural plasticity and neuropsychiatric disease. Nat. Rev. Neurosci. *19*, 215–234.

32. Peng, H., Xie, P., Liu, L., Kuang, X., Wang, Y., Qu, L., Gong, H., Jiang, S., Li, A., Ruan, Z., et al. (2021). Morphological diversity of single neurons in molecularly defined cell types. Nature *598*, 174–181.

33. Jiang, S., Wang, Y., Liu, L., Ding, L., Ruan, Z., Dong, H.-W., Ascoli, G.A., Hawrylycz, M., Zeng, H., and Peng, H. (2022). Petabyte-scale multimorphometry of single neurons for whole brains. Neuroinformatics *20*, 525–536.

34. Peng, H., Liu, Y., Jiang, S., Li, Y., Zhao, S., Yun, Z., Zhao, Z.-H., Zhang, L., Wang, G., and Chen, X. (2023). Full-Spectrum Neuronal Diversity and Stereotypy through Whole Brain Morphometry. Preprint at bioRxiv. ResearchGate. https://doi.org/10.21203/rs.3.rs-3146034/v1

35. Qu, L., Li, Y., Xie, P., Liu, L., Wang, Y., Wu, J., Liu, Y., Wang, T., Li, L., Guo, K., et al. (2022). Cross-modal coherent registration of whole mouse brains. Nat. Methods *19*, 111–118.

36. Wang, Q., Ding, S.-L., Li, Y., Royall, J., Feng, D., Lesnar, P., Graddis, N., Naeemi, M., Facer, B., Ho, A., et al. (2020). The Allen Mouse Brain Common Coordinate Framework: A 3D Reference Atlas. Cell *181*, 936–953.e20. https://doi.org/10.1016/j.cell.2020.04.007.

37. Grillo, F.W., Song, S., Teles-Grilo Ruivo, L.M., Huang, L., Gao, G., Knott, G.W., Maco, B., Ferretti, V., Thompson, D., Little, G.E., and De Paola, V. (2013). Increased axonal bouton dynamics in the aging mouse cortex. Proc. Natl. Acad. Sci. USA *110*, E1514–E1523.

38. Peters, A., and Feldman, M.L. (1976). The projection of the lateral geniculate nucleus to area 17 of the rat cerebral cortex. I. General description. J. Neurocytol. *5*, 63–84.

39. Li, Y., Wang, D., Ascoli, G.A., Mitra, P., and Wang, Y. (2017). Metrics for comparing neuronal tree shapes based on persistent homology. PLoS One *12*, e0182184.

40. Casas-Torremocha, D., Porrero, C., Rodriguez-Moreno, J., García-Amado, M., Lübke, J.H.R., Núñez, Á., and Clascá, F. (2019). Posterior thalamic nucleus axon terminals have different structure and functional impact in the motor and somatosensory vibrissal cortices. Brain Struct. Funct. *224*, 1627–1645.

41. Rodriguez-Moreno, J., Porrero, C., Rollenhagen, A., Rubio-Teves, M., Casas-Torremocha, D., Alonso-Nanclares, L., Yakoubi, R., Santuy, A., Merchan-Pérez, A., DeFelipe, J., et al. (2020). Area-specific synapse structure in branched posterior nucleus axons reveals a new level of complexity in thalamocortical networks. J. Neurosci. *40*, 2663–2679.

42. McElvain, L.E., Chen, Y., Moore, J.D., Brigidi, G.S., Bloodgood, B.L., Lim, B.K., Costa, R.M., and Kleinfeld, D. (2021). Specific populations of basal ganglia output neurons target distinct brain stem areas while collateralizing throughout the diencephalon. Neuron *109*, 1721–1738.e4.

43. Budd, J.M.L., Kovács, K., Ferecskó, A.S., Buzás, P., Eysel, U.T., and Kisvárday, Z.F. (2010). Neocortical Axon Arbors Trade-off Material and Conduction Delay Conservation. PLoS Comput. Biol. *6*, e1000711. https://doi.org/10.1371/journal.pcbi.1000711.

44. Nebel, M.E. (2000). On the Horton-Strahler number for combinatorial tries. RAIRO-Theor. Inf. Appl. *34*, 279–296.

45. Strahler, A.N. (1957). Quantitative analysis of watershed geomorphology. Eos Trans. Am. Geophys. Union *38*, 913–920.

46. Traag, V.A., Waltman, L., and Van Eck, N.J. (2019). From Louvain to Leiden: guaranteeing well-connected communities. Sci. Rep. *9*, 5233–5312.

47. Barabási, A.-L., and Albert, R. (1999). Emergence of scaling in random networks. Science *286*, 509–512.

48. Watts, D.J., and Strogatz, S.H. (1998). Collective dynamics of 'small-world' networks. Nature *393*, 440–442. https://doi.org/10.1038/30918.

49. Kleinberg, J.M. (1999). Authoritative sources in a hyperlinked environment. J. ACM JACM *46*, 604–632.

50. Liska, A., Galbusera, A., Schwarz, A.J., and Gozzi, A. (2015). Functional connectivity hubs of the mouse brain. Neuroimage *115*, 281–291.

51. Lord, L.-D., Stevner, A.B., Deco, G., and Kringelbach, M.L. (2017). Understanding principles of integration and segregation using whole-brain computational connectomics: implications for neuropsychiatric disorders. Philos. Trans. A Math. Phys. Eng. Sci. *375*, 20160283.

52. Holland, P.W., and Leinhardt, S. (1977). A method for detecting structure in sociometric data. In Social Networks (Elsevier), pp. 411–432.

53. Gal, E., London, M., Globerson, A., Ramaswamy, S., Reimann, M.W., Muller, E., Markram, H., and Segev, I. (2017). Rich cell-type-specific network topology in neocortical microcircuitry. Nat. Neurosci. *20*, 1004–1013.

54. Song, S., Sjöström, P.J., Reigl, M., Nelson, S., and Chklovskii, D.B. (2005). Highly nonrandom features of synaptic connectivity in local cortical circuits. PLoS Biol. *3*, e68.

55. Roy, D.S., Zhang, Y., Halassa, M.M., and Feng, G. (2022). Thalamic subnetworks as units of function. Nat. Neurosci. *25*, 140–153.

56. Goñi, J., Van Den Heuvel, M.P., Avena-Koenigsberger, A., Velez de Mendizabal, N., Betzel, R.F., Griffa, A., Hagmann, P., Corominas-Murtra, B., Thiran, J.-P., and Sporns, O. (2014). Resting-brain functional connectivity predicted by analytic measures of network communication. Proc. Natl. Acad. Sci. USA *111*, 833–838.

57. Poirazi, P., and Mel, B.W. (2001). Impact of active dendrites and structural plasticity on the memory capacity of neural tissue. Neuron *29*, 779–796.

58. Avena-Koenigsberger, A., Goñi, J., Betzel, R.F., van den Heuvel, M.P., Griffa, A., Hagmann, P., Thiran, J.-P., and Sporns, O. (2014). Using Pareto optimality to explore the topology and dynamics of the human connectome. Philos. Trans. R. Soc. Lond. B Biol. Sci. *369*, 20130530.

59. Baloyannis, S.J. (2009). Dendritic pathology in Alzheimer's disease. J. Neurol. Sci. *283*, 153–157.

60. Emoto, K. (2011). Dendrite remodeling in development and disease. Dev. Growth Differ. *53*, 277–286.

61. Huang, C.Y.-M., and Rasband, M.N. (2018). Axon initial segments: structure, function, and disease. Ann. N. Y. Acad. Sci. *1420*, 46–61.

62. Koleske, A.J. (2013). Molecular mechanisms of dendrite stability. Nat. Rev. Neurosci. *14*, 536–550.

63. Kweon, J.H., Kim, S., and Lee, S.B. (2017). The cellular basis of dendrite pathology in neurodegenerative diseases. BMB Rep. *50*, 5–11.

64. O'Keeffe, G.W., and Sullivan, A.M. (2018). Evidence for dopaminergic axonal degeneration as an early pathological process in Parkinson's disease. Parkinsonism Relat. Disord. *56*, 9–15.

65. Economo, M.N., Viswanathan, S., Tasic, B., Bas, E., Winnubst, J., Menon, V., Graybuck, L.T., Nguyen, T.N., Smith, K.A., Yao, Z., et al. (2018). Distinct descending motor cortex pathways and their roles in movement. Nature *563*, 79–84.

66. Winnubst, J., Bas, E., Ferreira, T.A., Wu, Z., Economo, M.N., Edson, P., Arthur, B.J., Bruns, C., Rokicki, K., Schauder, D., et al. (2019). Reconstruction of 1,000 projection neurons reveals new cell types and organization of long-range connectivity in the mouse brain. Cell *179*, 268–281.e13.

67. Rodriguez-Moreno, J., Rollenhagen, A., Arlandis, J., Santuy, A., Merchan-Pérez, A., DeFelipe, J., Lübke, J.H.R., and Clasca, F. (2018). Quantitative 3D ultrastructure of thalamocortical synapses from the "lemniscal" ventral posteromedial nucleus in mouse barrel cortex. Cereb. Cortex *28*, 3159–3175.

68. Brown, K.M., Sugihara, I., Shinoda, Y., and Ascoli, G.A. (2012). Digital morphometry of rat cerebellar climbing fibers reveals distinct branch and bouton types. J. Neurosci. *32*, 14670–14684.

69. De Paola, V., Holtmaat, A., Knott, G., Song, S., Wilbrecht, L., Caroni, P., and Svoboda, K. (2006). Cell type-specific structural plasticity of axonal branches and boutons in the adult neocortex. Neuron *49*, 861–875.

70. Karube, F., Kubota, Y., and Kawaguchi, Y. (2004). Axon branching and synaptic bouton phenotypes in GABAergic nonpyramidal cell subtypes. J. Neurosci. *24*, 2853–2865.

71. Chini, C.C.S., Peclat, T.R., Warner, G.M., Kashyap, S., Espindola-Netto, J.M., de Oliveira, G.C., Gomez, L.S., Hogan, K.A., Tarragó, M.G., Puranik, A.S., et al. (2020). CD38 ecto-enzyme in immune cells is induced during aging and regulates NAD+ and NMN levels. Nat. Metab. *2*, 1284–1304.

72. Clusella, P., Manubens-Gil, L., Garcia-Ojalvo, J., and Dierssen, M. (2024). Modeling the impact of neuromorphological alterations in Down syndrome on fast neural oscillations. Preprint at bioRxiv. https://doi.org/10.1101/2024.01.13.575481.

73. Manubens-Gil, L., Zhou, Z., Chen, H., Ramanathan, A., Liu, X., Liu, Y., Bria, A., Gillette, T., Ruan, Z., Yang, J., et al. (2023). BigNeuron: a resource to benchmark and predict performance of algorithms for automated tracing of neurons in light microscopy datasets. Nat. Methods *20*, 824–835.

74. Aerts, H., Fias, W., Caeyenberghs, K., and Marinazzo, D. (2016). Brain networks under attack: robustness properties and the impact of lesions. Brain *139*, 3063–3083.

75. Liu, L., Yun, Z., Manubens-Gil, L., Chen, H., Xiong, F., Dong, H.-W., Zeng, H., Hawrylycz, M., Ascoli, G., and Peng, H. (2023). Neuronal Connectivity as a Determinant of Cell Types and Subtypes. Preprint at bioRxiv. ResearchGate. https://doi.org/10.21203/rs.3.rs-2960606/v1

76. Krzywinski, M., Schein, J., Birol, I., Connors, J., Gascoyne, R., Horsman, D., Jones, S.J., and Marra, M.A. (2009). Circos: an information aesthetic for comparative genomics. Genome Res. *19*, 1639–1645.

77. Manubens-Gil, L. (2018). Computational and modeling approaches to multi-scale anatomical description of neuronal circuitry. PhD thesis (Universitat Pompeu Fabra).

78. Bria, A., Iannello, G., Onofri, L., and Peng, H. (2016). TeraFly: real-time three-dimensional visualization and annotation of terabytes of multidimensional volumetric images. Nat. Methods *13*, 192–194.

79. Wang, Y., Li, Q., Liu, L., Zhou, Z., Ruan, Z., Kong, L., Li, Y., Wang, Y., Zhong, N., Chai, R., et al. (2019). TeraVR empowers precise reconstruction of complete 3-D neuronal morphology in the whole brain. Nat. Commun. *10*, 3474–3479.

80. Ascoli, G., Mehta, K., Ljungquist, B., Ogden, J., Nanda, S., Ascoli, R., and Ng, L. (2023). Online Conversion of Reconstructed Neural Morphologies into Standardized SWC Format. Nat. Commun. *14*, 7429.

81. Sholl, D. (1953). Dendritic organization in the neurons of the visual and motor cortices of the cat. J. Anat. *87*, 387–406.

82. Costa, M., Manton, J.D., Ostrovsky, A.D., Prohaska, S., and Jefferis, G.S.X.E. (2016). NBLAST: rapid, sensitive comparison of neuronal structure and construction of neuron family databases. Neuron *91*, 293–311.

83. Erdős, P., and Rényi, A. (1960). On the evolution of random graphs. Publ Math Inst Hung Acad Sci *5*, 17–60.

84. Blondel, V.D., Guillaume, J.-L., Lambiotte, R., and Lefebvre, E. (2008). Fast unfolding of communities in large networks. J. Stat. Mech. *2008*, P10008.

85. Floyd, R.W. (1962). Algorithm 97: shortest path. Commun. ACM *5*, 345.

86. Roy, B. (1959). Transitivité et connexité. Comptes Rendus Hebd. Seances Acad. Sci. *249*, 216–218.

87. Warshall, S. (1962). A theorem on boolean matrices. J. ACM. *9*, 11–12.

STAR★METHODS

KEY RESOURCES TABLE

REAGENT or RESOURCE	SOURCE	IDENTIFIER
Deposited data		
Bouton data	Peng et al.[34]	https://drive.google.com/drive/folders/1NwwTe840_0KQhv-zVLhw58LU9nntkb-F
Software and algorithms		
Topological Morphology Descriptor (TMD)	Kanari et al.[30]	https://github.com/BlueBrain/TMD
Navis 1.3.0	navis-org	https://github.com/navis-org/navis
igraph 0.9.9	igraph development team	RRID: SCR_019225
Circos 0.6.9	Krzywinski et al.[76]	RRID: SCR_011798
Leidenalg 0.8.9	Traag et al.[46]	https://github.com/vtraag/leidenalg
Network analysis	Manubens-Gil, L.[77]	http://hdl.handle.net/10803/664511
Python 3.9.7	Python Software Foundation	RRID: SCR_008394
Scripts for analysis	This paper	https://zenodo.org/doi/10.5281/zenodo.10617785
Other		
Neuron related information	Peng et al.[32]	https://doi.org/10.1038/s41586-021-03941-1
Additional Data	This paper	https://doi.org/10.5281/zenodo.8216366

RESOURCE AVAILABILITY

Lead contact

Further information and requests for resources and code should be directed to and will be fulfilled by the lead contact, Linus Manubens-Gil (linusmg@seu.edu.cn).

Materials availability

This study did not generate new unique reagents.

Data and code availability

- **Data:** All original data including full neuron reconstructions, together with observed bouton locations can be found at: https://drive.google.com/drive/folders/1NwwTe840_0KQhv-zVLhw58LU9nntkb-F The additional data including: full names of all cell types involved, acronyms, number of neurons, and average bouton density; comparison between the bouton density calculated from our data and other articles; Statistical tests in Figure 3, including correlation and independence statistical test of degree distribution and triad census among different networks; network analysis results: average path length, clustering coefficient, hubs and authorities scores and triad census; can be found at https://doi.org/10.5281/zenodo.8216366.
- **Code:** All versions of original code can be found at https://zenodo.org/doi/10.5281/zenodo.10617785.
- **Additional information:** Any other additional information required to reanalyze the data reported in this paper is available from the lead contact upon request.

METHOD DETAILS

Sources of experimental data

Recent advances in light microscopy allowed the generation of complete neuronal reconstructions at micrometric resolution. Here, we used 1891 full neuron reconstructions data with axonal bouton locations from a dataset obtained at SEU-Allen.[32] The data was generated using the MorphoHub platform,[33,34] which follows a multi-level annotation protocol that we describe briefly: First, the neuronal reconstruction is delineated using Vaa3D Terafly[78] and TeraVR,[79] being cross-checked by at least two annotators. Then, we used a four-step approach to extract bouton data automatically. Firstly, the neuronal tree representation of L2 data is resampled using a fixed-length interval. In this work, the interval is set to be 4 μm. Secondly, for each node in the neuronal tree, the corresponding image intensity value is retrieved from the whole brain datasets. Since the nodes cannot be guaranteed to locate at the centers of the putative boutons, the nodes can be locally shifted to the maximum intensity position within a small area (e.g., 2 voxels). We

assume that the intensity of imaging signal along axons obeys the 1-D Gaussian distribution and a bouton site tends to have intensity jump compared with its neighboring nodes. Thus, the third step is to calculate the intensity jump threshold for each small image block (e.g., 128 × 128x123) as the standard deviation of the block, and extract bouton candidate in a block-wise manner. Finally, we remove any possible duplicates by deleting boutons at a distance closer than 5 voxels.[34] We have presented an example of bouton detection from 3D images in Figure S1C. According to our previous statistics, random inspection of the results indicated that the bouton detection precision was above 95%. We also found that nearly 80% of the average spacing of adjacent boutons along an axon ranged from 5 to 20μm. For more details, please refer to this paper[33] for information about the specific bouton detection process, and to this recent preprint[34] for further anatomical analyses and data validation. Putative bouton locations are stored as an extra column in extended Stockley-Wheal-Cole (ESWC) files describing the neuron morphology.[80]

The SEU-ALLEN dataset has a total of 1891 neurons suitable for predicting bouton locations. The dataset includes 97 cell types defined by the brain region where their soma is located (s-types; see supporting datasets of glossary in the Data Availability section). The reconstructions have been obtained from 39 brains and are equally distributed between the left and right hemispheres. After annotation of the full neuronal structure, the trees have been spatially registered to CCFv3.[35]

Calculation of bouton distribution

Since downsampling was used to reduce the file size after the boutons were identified, we resampled the ESWC files at an interval of 10 μm. We measured the distribution of bouton and axon length through the full axonal tree using the Sholl analysis on the neuron reconstructions before registration to CCFv3. The Sholl Analysis is the process of measuring neuron properties in concentric circles around the soma, and it provides a quantitative description of morphological features for the analyzed neurons.[81] We measured the number of branches intersecting each circle and both cable length and number of axon boutons between consecutive circles at 100 μm intervals. To do so, we used the "sholl_analysis" function of the Navis package (version 1.3.0)[82] in Python (version 3.9.7).

To validate the observed densities of boutons and to be able to compare to experimental measurements obtained with electron microscopy, we obtained average bouton densities (number of boutons per micrometer of axon length) for all axons located in specific CCFv3 regions. We obtained the total number of observed boutons and divided by the total axon length in each region.

To test the impact of the inhomogeneous observed bouton distributions on the network structure, we generated model neurons with homogeneous bouton densities. Given that different s-types showed diverse observed bouton distributions, we obtained the average bouton density for each s-type. To do so, we scaled the average axon length distribution of each s-type within a scaling factor representing bouton density in a range between 0 and 1 with steps of 0.001. 0 would imply no boutons at all throughout the tree, and 1 would imply one bouton for every micron of axonal length. We chose the scaling factor value that minimized the squared difference to the observed bouton distribution based on our experimental data. Given that these average bouton densities could be useful for generating connectivity in models of cortico-thalamic circuits the obtained values can be found in the supporting datasets in the Data Availability section.

To simulate a uniform distribution of axonal boutons in the individual reconstructions according to the average density of each s-type, we devised an algorithm to define axon bouton locations synthetically. Specifically, first, we found all end nodes of all branches, which are leaf nodes and backtracked from these leaf nodes sequentially. In the process of backtracking, boutons were set at equal intervals defined by the inter-bouton distance determined by the inverse of the average bouton density. To prevent repeated assignment of boutons in low-order branches, paths that had already been traversed were not visited again.

To compare with the bouton density in previous experimental studies, we counted the total axon length and the bouton number from neurons with specific soma regions within any brain region in the CCFv3 model. The number of boutons per unit distance was obtained by dividing the two values. But such a result tends to underestimate the bouton density because boutons are not evenly distributed over the axon.

Generation of networks

Given that our full neuron reconstructions and bouton data are spatially registered to the mouse CCFv3, the neuronal morphologies can be explored in the same coordinate space, allowing us to explore the colocalization of axonal boutons and dendritic trees. We developed an algorithm to obtain a whole brain connectivity matrix at the single-cell level based on our dataset. In the resulting network, nodes are single neurons and edges are the connection strength between a pair of neurons *i* and *j*. According to Peters' rule,[38] whether two neurons are connected can be determined by the presence of a nearby axon and dendrite. Here, we used a nuanced Peters' rule[27] given that the potential connectivity is weighted by the number of boutons on such an axon-dendrite connection pair.

Specifically, first, we divided the whole brain into 30*30 μm cubes and calculated the axon length, dendrite length, and bouton number of each neuron within each cube. We respectively calculated the network obtained when cube size was 1, 5, 10, 30 and 50 μm. Their number of nodes and edges are Cube = 1μm, N = 238, E = 150; Cube = 5μm, N = 1520, E = 3362; Cube = 10μm, N = 1680, E = 7241; Cube = 30μm, N = 1781, E = 14056; Cube = 50μm, N = 1814, E = 18235. We chose the minimum resolution that guarantees enough nodes and edges. And this is consistent with our recognition of the errors generated during the alignment process.

We considered that when both axons and dendrites are present in a cube with existing boutons, there is a potential connection. We defined the connection strength based on the number of boutons in each cube (Equation 1). Given that multiple pre- and postsynaptic

neuron segments may coexist in each cube, we distributed the total number of observed boutons to all dendrites in the cube according to the proportion of dendrite length contributed by each neuron. We assumed that spines are uniformly distributed on the dendrite, and therefore the length of the postsynaptic dendrite can be used as a proxy for the number of synaptic contacts. Thus, the multiplication of the number of boutons and the proportion of the dendrite length in a cube can be considered as the connection strength. This provides all pairwise connection strengths between pre- and postsynaptic neurons in each cube. By iterating this process through the whole brain, a full single-cell connectivity matrix is obtained.

The three networks used for comparison: the random network, the small-world network and the scale-free network, can be generated directly by the functions in Igraph: "Erdos_Renyi()",[83] "Watts_Strogatz()",[48] "Barabasi()".[47] For the random network, we keep the number of nodes and edges the same as for the *observed* network. For the small-world network, we set the dimension of the lattice to 1 and choose the rewiring probability to be 0.02. The size is the number of nodes in *observed* network. And the number of edges is adjusted by giving the distance (number of steps) within which two vertices will be connected to make that as close as possible to the *observed* network. Finally, the extra edges are removed randomly. Similarly, for the scale-free network, we adjust the number of outgoing edges generated for each vertex to approximate the *observed* network while keeping the number of nodes the same, and finally remove the excess edges randomly as well.

Network analysis

To quantify network structural properties, we obtained the degree distribution, triad census, hubs, and authorities using the "igraph" package (version 0.9.9) in Python (version 3.9.7). Correspondingly, this toolkit provides these functions: "degree_distribution()", "triad_census()", "authority_score()", "hub_score()", which we used with default parameters. We generated circular plots to visualize the networks using Circos[76] (version 0.6.9).

Community detection

To explore the community structure of the networks, we used the Leiden algorithm,[46] which is an optimization of Louvain's clustering method[84] that ensures detected communities are connected and have faster computation. Specifically, the Leiden algorithm divides the graph nodes into communities while optimizing modularity in three phases: (1) local assignment of nodes into communities, (2) refinement of the partition, and (3) aggregation of the network reducing the number of nodes to represent communities. Here we used the "leidenalg" package[46] (version 0.8.9) in Python (version 3.9.7), and to ensure that the analyzed communities had enough nodes, we arbitrarily selected the largest six groups for subsequent analysis and especially to generate the simple plots accounting for the major communities in each network.

Multi-objective optimality metrics

Considering that the basic function of a neural network is the transmission and storage of information and that building a network has a material and metabolic cost, we use three quantities to explore putative functional constraints of the network: cost, storage capacity, and routing efficiency.[77]

Cost

Cost is defined as the number of boutons in the network.

$$C = \sum_{i,j=1}^{N} nb_{i,j} \quad \text{(Equation 2)}$$

where $nb_{i,j}$ is the number of boutons connecting a pair of neurons i and j, and N is the total number of neurons in the network.

Storage capacity

We estimated the storage capacity of a network as the sum of the total number of non-redundant possible states for each neuron receiving s connections provided by d pre-synaptic neurons as previously defined by Poirazi and Mel for linear neurons.[57] Briefly, the combinatorial "n choose k" quantification of possible states for a post-synaptic neuron expressed in bits (basic unit of information) is given by:

$$b_L = 2log_2 \frac{s+d-1}{s} \quad \text{(Equation 3)}$$

and total storage capacity of the network by:

$$B_L = \sum_{i=1}^{N} 2log_2 \frac{s_i+d_i-1}{s_i} \quad \text{(Equation 4)}$$

Where N is the number of nodes in the network.

Routing efficiency

Routing efficiency is inversely proportional to the weighted shortest path length φ_{ij} in the network between any pair of nodes (neurons) i and j. When two neurons in the network are closely connected or have more synapses, the path length between them is reduced, and the routing efficiency increases. We obtained the shortest path length matrices using an in-house implementation of the Floyd-Warshall algorithm.[85–87] The formal definition for the routing efficiency is as follows:

$$E_{rout} = \sum_{ij} \frac{1/\varphi_{ij}}{N(N-1)}, i \neq j \quad \text{(Equation 5)}$$

Where φij is the graph shortest path length between the nodes i and j, and N is the total number of nodes in the graph.

Perturbation

To study the effect of putative biologically realistic[1] morphological perturbations on the network, we designed three perturbation operations: scaling of neuron size, pruning of neuron branches, and removal of synaptic boutons. We used those to perturb morphological details of the neurons, including their size, complexity of the neurites, and number of boutons.

Scaling of neuron size

This operation involves reducing the size of the axonal, dendritic tree, or entire neuron by a factor ranging from 0.5 to 0.9 in intervals of 0.1. For dendrite scaling, we select dendritic branches and scale the 3D spatial coordinates of all points forming the branches relative to the coordinates of the soma. Since all dendritic branches in our data are connected to the soma, we can accurately scale their coordinates. For axon scaling, we identify the longest axon branch as the projection branch and keep it unmodified. Then, we scale the coordinates of the axon subtrees relative to the point of connection to the projection branch.

To separately study the impact of bouton distribution and axonal tree complexity, we adjust the number of boutons when scaling axons. Bouton locations are assigned to specific nodes in the neuron tracings. In the case of uniform distribution, we reset the position of the boutons in the scaled axon according to the bouton density per unit of axon length. In the case of observed boutons, we first calculate the distance between each consecutive pair of boutons and sort them from smallest to largest. The number of boutons to be deleted is determined based on the scaling ratio, and the boutons are uniformly deleted from the distance-ordered list. This procedure ensures that the distribution of boutons per unit of length remains unchanged after scaling the axonal tree size.

Pruning of neurites

Neurite pruning refers to the process of deleting a certain percentage of dendritic or axonal branches to modify the neuron morphology. In our study, we performed various types of perturbations by removing only the axonal, dendritic branches, or both. First, we identified the number of leaf nodes (termination points) in a given neuron. We then selected a set of leaf nodes based on a pruning ratio ranging from 0.5 to 0.9 in 0.1 intervals. The pruning of single branches began from one of the selected leaf nodes and proceeded through parent nodes until the first branch node was encountered, and all nodes in the path were deleted.

Removal of boutons

The process of removing boutons randomly does not alter the neuron morphology but only deletes a fixed percentage of boutons. We start by identifying the total number of boutons in a neuron, after which we select boutons randomly at a fixed proportion range between 0.5 and 0.9 in 10% intervals. We label the selected points as axonal continuation points, which signifies that the reassigned nodes are not considered while generating connectivity matrices to establish connections.

QUANTIFICATION AND STATISTICAL ANALYSIS

Sample size of different neuron numbers is described in the results section either in the main text or figure legends. We tested putative and random bouton distribution statistical differences using the one-way Analysis of Covariance (ANCOVA). We used pairwise t-tests for all Sholl analysis differences in bouton distribution and bouton density of regions. Considering that the degree distribution and triad motifs of the network are not Gaussian with order and outliers, we used two-sample Kolmogorov-Smirnov tests for the independence test and Spearman correlation to show the correlation. We used pairwise t test for hub scores. We considered statistical results to be significant when $p < 0.05$. We plotted as mean ± standard error of the mean or ±standard deviation. For network random instantiations and perturbations, we performed ten repetitions. All the analyses were performed using Python (version 3.9.7) and its packages scipy (version 1.7.3).